

**Vortex arrays as emergent collective phenomena for circle swimmers**

A. Kaiser and H. Löwen\*

*Institut für Theoretische Physik II: Weiche Materie, Heinrich-Heine-Universität Düsseldorf,  
Universitätsstraße 1, D-40225 Düsseldorf, Germany*

(Received 3 December 2012; published 15 March 2013)

Collective properties of many rodlike circle swimmers are explored by computer simulations in two spatial dimensions. In the model considered, the center of mass of a single swimmer moves on a circle with radius  $R$ . Therefore, the model provides an interpolation between an interacting self-propelled-rod model for linear swimmers ( $R \rightarrow \infty$ ) and that of interacting passive rotors ( $R = 0$ ). We map out the state diagram for various swimmer densities and radii  $R$ . For increasing density, the dilute state is followed by vortices consisting of single particles (singlet-vortex state), where neighboring particles are perpendicularly oriented, and vortices of swimmer pairs (doublet-vortex state). The vortices exhibit strong structural ordering on an array. At higher densities, a slowed rotor fluid with a significant degree of mutual rotation hindrance occurs. The single-particle vortex structure becomes unstable above a threshold in the circling radius  $R$ , while pair vortices are stable only for intermediate radii  $R$ . A simple theory is proposed to predict the topology of the state diagram. Our results are verifiable for bacterial and artificial rodlike circle swimmers.

DOI: [10.1103/PhysRevE.87.032712](https://doi.org/10.1103/PhysRevE.87.032712)

PACS number(s): 87.15.A-, 82.70.Dd, 61.30.-v, 61.20.Lc

**I. INTRODUCTION**

Both swimming micro-organisms [1,2] and synthetic colloidal swimmers [3] are able to form remarkable collective spatiotemporal patterns [4–10] including swarming [11–14] and complex swirling [15–24] behavior. Most of the observed patterns can be obtained by a simple modeling that includes the tendency of the particles to move autonomously and their direct interaction mainly governed by the excluded volume of effective anisotropic objects [20,25]. When supplemented with Brownian dynamics, binary collisions between neighboring particles lead to mutual alignment and thus provide a mechanism of swarming [26]. The observed effects occur in most cases in two dimensions, i.e., for particles moving in a planar geometry.

In fact, self-propelled particles in two dimensions can be realized in a number of ways including autonomously navigating confined bacteria and microbes [16,17,27–30], polar granular rods on a vibrating flat surface [31,32], flagellated alga [33], and even pedestrians in a pedestrian zone [34,35]. Moreover, colloidal dispersions have been shown to provide various valuable model systems of active matter [36–43]. Most of these particles have an anisotropic rodlike shape and move along their orientation axis such that a single particle proceeds along a line. This is a key ingredient in previous modeling of many swimmers [14,26,44–49].

Moreover, self-propelled particles have been discovered that move in circles rather than in a straight line. Examples for these circle swimmers include various bacteria [50–55], protozoans [56], microtubules [57], spermatozoa [18,58,59], crustaceans [60], and spherical camphors that have been shown to exhibit circular swimming at an interface [61]. Furthermore, synthetic microswimmers with various shapes exhibit circular motion [62–65]. Driven Brownian particle models [66–70] have been proposed to describe the basic physics of circle

swimmers where the particles proceed with both an effective translational and angular propagation velocity and experience additional Brownian fluctuations. The deterministic (noise-free) trajectory in two dimensions is a closed circle. More explicit models that resolve the swimming strokes have recently been put forth for single circle swimmers [71,72].

However, the collective properties of circle swimmers at finite density are rarely understood. Experiments [18] have shown emerging dynamic arrays of vortices for spermatozoa resembling quantized rotating waves if the density exceeds a threshold. The origin was explained in terms of hydrodynamic interactions. However, apart from a coarse-grained recent diffusive theory [73], there is no particle-resolved simulational study nor any theoretical study for the emergent behavior of many circle swimmers. Here we simulate the collective behavior of many circle swimmers by a minimal model in two spatial dimensions incorporating excluded volume interactions. The swimmers are interacting via a strongly repulsive and short-range Yukawa-segment potential [74], which prevents particles from overlapping. Each rod has a length  $\ell$ . The self-motility of the individual swimmers is imposed by introducing a constant translational velocity along the main orientation axis of each rod and a constant angular velocity that rotates each rod. The combination of both translational and rotational self-propulsion results in a circular swimming path for the center of mass of radius  $R$  for each individual rod. At finite density, different circle swimmers will collide, leading to nontrivial emergent behavior that gets crowded and nontrivial if the area  $\pi R^2$  embraced by a single swimmer is occupied on average by two or more swimmers. In particular, at intermediate and high densities, novel emerging effects are expected.

The model considered here has been studied previously in two special limits, namely, for vanishing angular velocity [20,25] and vanishing translational velocity [75]. For vanishing angular velocity, we recover the special case of linear swimmers that move in straight lines corresponding to the limiting case  $R \rightarrow \infty$ . Even though the averaged swimming

\*hlowen@thphy.uni-duesseldorf.de

direction is constant, it has been shown [20,25] that at finite density, swirls emerge in the model. The average rotational sense of the swirls, however, averages to zero due to symmetry. The complementary case of vanishing translational velocity [75,76] describes passive rotors. The absence of translational propulsion leads to a vanishing swimming radius  $R$ . These rotors can be realized by placing passive colloids into circularly polarized light fields [77–79]. Passive rotors have been shown to exhibit a  $T$  structure of neighboring rotating rods that can also be viewed as a special kind of vortex array, a singlet vortex, in the sense that each rotor forms its own vortex and neighboring vortices possess perpendicular rod orientation. The compact though dynamic  $T$  structure is formed since mutual collisions are avoided. At high density, the vortex array structure disappears due to jamming [75], leaving a slowed rotor fluid as the high-density state.

In our simulation of many circle swimmers, we have the radius  $R$  of a single swimmer's path as an additional parameter. First we confirm that the singlet-vortex phase and the slowed rotor fluid phase that were discovered previously for vanishing  $R$  [75] possess a large stability for finite  $R$ . More surprisingly, we find a different vortex array formation at intermediate swimmer densities and an intermediate range of radii  $R$ . In this phase, the vortices are composed of circle swimmer pairs that are oriented antiparallel with respect to each other. Many of these doublet vortices exhibit strong structural ordering on an array. We propose a simple theory to predict the onset of circle swimmer pairing to understand the underlying mechanisms for vortex array formation. Our vortex array is induced by steric interactions together with circular self-propulsion and is therefore different in origin that the hydrodynamically induced vortices of Refs. [18,80]. The rotation sense of the vortices is obviously correlated with the sense of rotation of a single swimmer since the clockwise or counterclockwise symmetry of rotation is broken in our model. This makes our vortex pairing different from previous explorations of swirling in linear swimmers at intermediate densities [16,17,20,81,82]. In principle, our results are verifiable for bacterial and artificial rodlike circle swimmers.

The paper is organized as follows. In Sec. II we specify our model for circle-swimming self-propelled rods, the corresponding equations of motion, and the simulation technique. Simulation results on the nonequilibrium state diagram are presented and analyzed in Sec. III, while in Sec. IV a simple theory is proposed to predict the vortex formation. We conclude in Sec. V with a brief discussion of possible extensions of the model and highlight opportunities to observe the predicted behavior in experiment.

## II. FRICTIONAL DYNAMICS OF A SELF-PROPELLED-ROD MODEL

The rodlike circle swimmers in our model are characterized by a length  $\ell$  and are driven by a constant self-propulsion force  $F$  directed along the main rod axis  $\hat{\mathbf{u}}$ . The actual position of the  $\alpha$ th rod ( $\alpha = 1, \dots, N$ ) is described by a center of mass position vector  $\mathbf{r}_\alpha$  and a unit orientational vector  $\hat{\mathbf{u}}_\alpha = (\cos \varphi_\alpha, \sin \varphi_\alpha)$ . We do not resolve the details of the swimming mechanism. The force  $F$  is a formal one that results in some overdamped dynamics in a constant propagation

velocity as in previous models [25,45,83]. Similarly, the circular movement is implemented using an additional torque  $\mathbf{M}$  normal to the plane of motion as described for a single rod in Ref. [66]. The repulsive rod forces are described by a Yukawa-segment interaction, which is an established model for charged rodlike colloids [84,85], as suspensions of the tobacco-mosaic virus [74,86] and DNA strands [87,88]. In detail, each rod is discretized into  $n$  spherical segments and a repulsive Yukawa force with characteristic screening length  $\lambda$  between the segments of different rods is imposed. Thereby each rod of length  $\ell$  has a defined diameter  $\lambda$  [74]. The segments are distributed equidistantly along the rod axis with a fixed distance  $d = \ell / [(n + 1)(n - 1)]^{1/2} \leq \lambda$ .

The total pair potential between a rod pair  $\alpha$  and  $\beta$  with orientational unit vectors  $\{\hat{\mathbf{u}}_\alpha, \hat{\mathbf{u}}_\beta\}$  and center of mass distance  $\Delta\mathbf{r}_{\alpha\beta} = \mathbf{r}_\alpha - \mathbf{r}_\beta$  is given by

$$U_{\alpha\beta} = \frac{U_0}{n^2} \sum_{i=1}^n \sum_{j=1}^n \frac{\exp[-(r_{ij}^{\alpha\beta}/\lambda)]}{r_{ij}^{\alpha\beta}}, \quad (1)$$

where  $U_0$  is an amplitude and

$$r_{ij}^{\alpha\beta} = |\Delta\mathbf{r}_{\alpha\beta} + (l_i\hat{\mathbf{u}}_\alpha - l_j\hat{\mathbf{u}}_\beta)| \quad (2)$$

is the distance between the  $i$ th segment of rod  $\alpha$  and the  $j$ th segment of rod  $\beta$ , with  $l_i \in [-(\ell - \lambda)/2, (\ell - \lambda)/2]$  denoting the position of segment  $i$  along the symmetry axis of the rod  $\alpha$  (see Fig. 1). We introduce an aspect ratio  $p = \ell/\lambda$  to quantify the effective anisotropy of the rod-shaped particles. The number of segments per rod is defined by  $n = \lfloor 9p/8 \rfloor$ , with  $\lfloor \cdot \rfloor$  denoting the nearest integer.

We focus on the overdamped regime in the low-Reynolds-number limit, which is the relevant one for micro-organisms and artificial self-propelled colloidal mesogens. The resulting

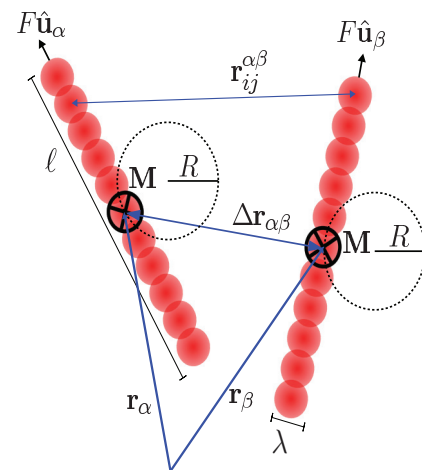


FIG. 1. (Color online) Sketch of a pair of rodlike circle swimmers with  $n = 11$  repulsive Yukawa segments and aspect ratio  $p = \ell/\lambda$ . Self-propulsion is provided by a constant force  $F$  acting along the main rod axis  $\hat{\mathbf{u}}$ . The circular motion is brought about by an additional torque  $\mathbf{M}$  perpendicular to the plane of motion. The total rod pair potential is obtained by a sum over all Yukawa segment pairs with distance  $r_{ij}^{\alpha\beta}$  and is a function of the center of mass distance vector  $\Delta\mathbf{r}_{\alpha\beta}$  and orientations (1). The circular swimming path of radius  $R$  of the center of mass coordinates is also indicated.

equations of motion for the center of mass position  $\mathbf{r}_\alpha(t)$  and orientation  $\hat{\mathbf{u}}_\alpha(t) = [\cos \varphi_\alpha(t), \sin \varphi_\alpha(t)]$  of the circle swimmer emerge from a balance of the forces and torques acting on each rod  $\alpha$  and are similar to those described in Ref. [25]:

$$\mathbf{f}_T \cdot \partial_t \mathbf{r}_\alpha = -\nabla_{\mathbf{r}_\alpha} U + F \hat{\mathbf{u}}_\alpha, \quad (3)$$

$$\mathbf{f}_R \cdot \partial_t \hat{\mathbf{u}}_\alpha = -\nabla_{\hat{\mathbf{u}}_\alpha} U + \mathbf{M}. \quad (4)$$

Here  $F$  is the constant self-motility force acting along the longitudinal axis of each rod (Fig. 1),  $U = (1/2) \sum_{\beta, \alpha; \beta \neq \alpha} U_{\alpha\beta}$  is the total potential energy,  $\nabla_{\hat{\mathbf{u}}}$  denotes the gradient on the unit circle, and

$$\mathbf{f}_T = f_0 [f_{\parallel} \hat{\mathbf{u}}_\alpha \hat{\mathbf{u}}_\alpha + f_{\perp} (\mathbf{I} - \hat{\mathbf{u}}_\alpha \hat{\mathbf{u}}_\alpha)], \quad (5)$$

$$\mathbf{f}_R = f_0 f_R \mathbf{I} \quad (6)$$

are the translational and rotational friction tensors ( $\mathbf{I}$  is the two-dimensional unit tensor) with a Stokesian friction coefficient  $f_0$ . The dimensionless geometric factors  $\{f_{\parallel}, f_{\perp}, f_R\}$  depend solely on the aspect ratio  $p$  and we adopt the standard expressions for rodlike macromolecules, as given in Ref. [89],

$$\frac{2\pi}{f_{\parallel}} = \ln p - 0.207 + 0.980p^{-1} - 0.133p^{-2}, \quad (7)$$

$$\frac{4\pi}{f_{\perp}} = \ln p + 0.839 + 0.185p^{-1} + 0.233p^{-2}, \quad (8)$$

$$\frac{\pi p^2}{3f_R} = \ln p - 0.662 + 0.917p^{-1} - 0.050p^{-2}. \quad (9)$$

The additional torque  $M$  induces a circular motion of a single swimmer with a radius

$$R = \frac{f_R F}{f_{\parallel} M} \quad (10)$$

and an angular velocity

$$\omega_0 = \frac{M}{f_R}. \quad (11)$$

Clearly, there is no finite temperature in our model as any stochastic fluctuations are ignored.

In our simulations, we have adopted characteristic units such that  $\lambda = 1$ ,  $F = 1$ , and  $f_0 = 1$ , which means that distance is measured in units of  $\lambda$ , velocity in units of  $F/f_0$ , time in units of  $\tau_0 = \lambda f_0 / F$ , and energy in units of  $F\lambda$ . Upon rescaling to dimensionless coordinates, four relevant system parameters remain: the dimensionless Yukawa amplitude  $\tilde{U}_0 = U_0 / F\lambda$ , which determines the hardness of the rod interactions relative to their characteristic propulsion energy, the aspect ratio  $p$ , the reduced radius  $R/\lambda$ , and the packing fraction of the rods. This fraction is specified in terms of the dimensionless area fraction

$$\eta = \frac{\pi}{4} \frac{N}{A} \ell^2, \quad (12)$$

where  $N$  is the total number of rodlike circle swimmers and  $A$  denotes the area of the quadratic simulation box. For steeply repulsive Yukawa interactions, the general dynamical behavior resembles that of hard rods and only weakly depends on the Yukawa amplitude and we set  $\tilde{U}_0 = 250$ . We further consider anisotropic rods with fixed aspect ratio  $p = 10$ . The remaining quantities, the reduced swimmer radius  $R/\lambda$  and area fraction

$\eta$ , constitute the main steering parameters for our investigation. We simulate the evolution of the many-body self-propelled rod model as a function of time  $\tau = t/\tau_0$  in a square box with periodic boundary conditions at packing fractions in the range  $0.1 < \eta < 2.5$ . The simulations are carried out using a total number of  $N = 10^3$  rods. Initial configurations are generated from a rectangular lattice of aligned rods with  $\hat{\mathbf{u}}$  pointing randomly up or down. The rods are randomly displaced from the initial lattice such that the starting configuration bears already some randomness. We have tested different random starting configurations and confirmed that the steady state properties do not depend on the starting configuration. We then relax the system during an time interval of a transitory time  $\tau_T = 2000$  before statistics are being gathered over an interval  $\tau_S = 40000$ . We checked that the results do not depend on  $\tau_T$  if  $\tau_T$  is chosen larger than 2000. Moreover, we have done longer exploration runs with  $\tau_S = 100000$  to confirm that the steady state averages are reproduced. Finally, we have checked the system size dependence by systematically exploring particle numbers in the range of  $N = 100$ – $1000$  particles. The occurrence of the different states is stable.

### III. SIMULATION RESULTS

Figure 2(a) shows a state diagram for rodlike circle swimmers in the two-dimensional parameter space of swimmer density  $\eta$  and swimming radius  $R$ . Four different states emerge, for which typical simulation snapshots are shown in Figs. 2(b)–2(e) (see also Ref. [90]). We discriminate between different states by suitable order parameters as explained in detail below, but emphasize here that there are no strict phase transitions between the different states. Let us first discuss the contents of Fig. 2 before we characterize the states in more detail.

For low densities there are only very few collisions and therefore little or no collective motion. Consequently, there is a dilute state at low density  $\eta$  [see Fig. 2(b)]. Complementarily, at high density, there is a slowed rotor fluid with no particular mesostructure [see Fig. 2(e)]. In this state, rotating rods collide, which slows down their mean angular velocity. More interestingly, there are intervening phases at intermediate densities. We find two different vortex array states. The first consists of singlet vortices such that every vortex comprises a single particle. This phase has been called the  $T$  structure in earlier investigations for passive particles at vanishing radius  $R$  [75] since it clearly shows a perpendicular orientation of neighboring rods. We refer to this state here as a singlet-vortex array phase as every particle rotates around its own such that any vortex comprises a single particle [see Fig. 2(c)]. The second phase is a doublet-vortex array such that each vortex comprises two rods that are oriented in an antiparallel way. The rod pairing is clearly visible in the snapshot shown in Fig. 2(d). It is important to note that the doublet-vortex state is stable only in a finite range of swimming radii  $\lambda/2 < R < 7\lambda$ . Its transition density towards the slowed rotor fluid exhibits a large nonmonotonicity in  $R$ , which implies a marked reentrant behavior of the slowed rotor fluid if  $R$  is increased at fixed density. For the parameter space studied, we never found vortices with more than two rods.

In more detail, we now define order parameters in order to distinguish and characterize the four different states.

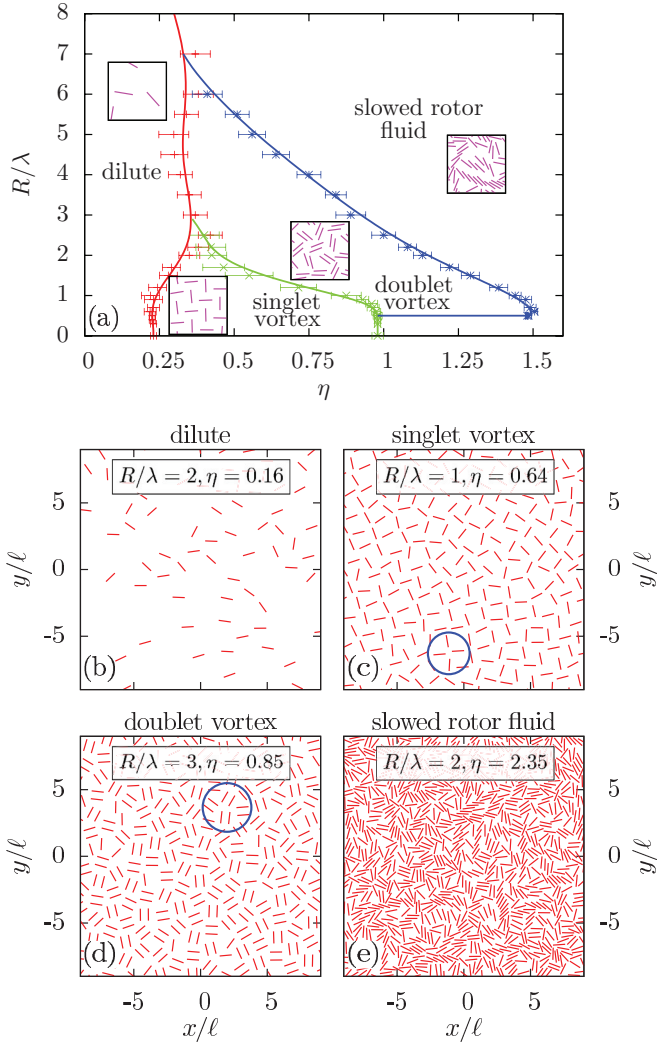


FIG. 2. (Color online) (a) Nonequilibrium state diagram of rodlike circle swimmers in the parameter space spanned by the swimming radius  $R$  and the swimmer density  $\eta$ . Four different states emerge, which are depicted as dilute for low swimmer densities, singlet vortex for intermediate densities and low rotation radii, doublet vortex for higher swimmer densities, and slowed rotor fluid for even higher densities. (b)–(e) Characteristic simulation snapshots for the four states are also shown, including (blue) circles to show typical configurations of the vortex array states.

To analyze the orientation of neighboring rods we define normalized orientational order parameters

$$m_1 = \langle \cos \theta(r) \rangle_a, \quad (13)$$

$$m_2 = \langle \cos^2 \theta(r) \rangle_a, \quad (14)$$

where  $\langle \dots \rangle_a = \int_0^a dr g(r) \dots / \int_0^a dr g(r)$  is a statistical steady state average. These order parameters correspond to measures of the polar and nematic order in a neighbor shell of size  $a$ . Here  $g(r)$  is the pair correlation function between two rods (provided their center of mass positions have a distance  $r$ ) and  $\theta(r)$  denotes the angle between their orientations. Moreover,  $a = (N/A)^{-1/2}$  is the average distance between two rods. The order parameter  $m_2$  was already applied to evaluate passive rotors [75].

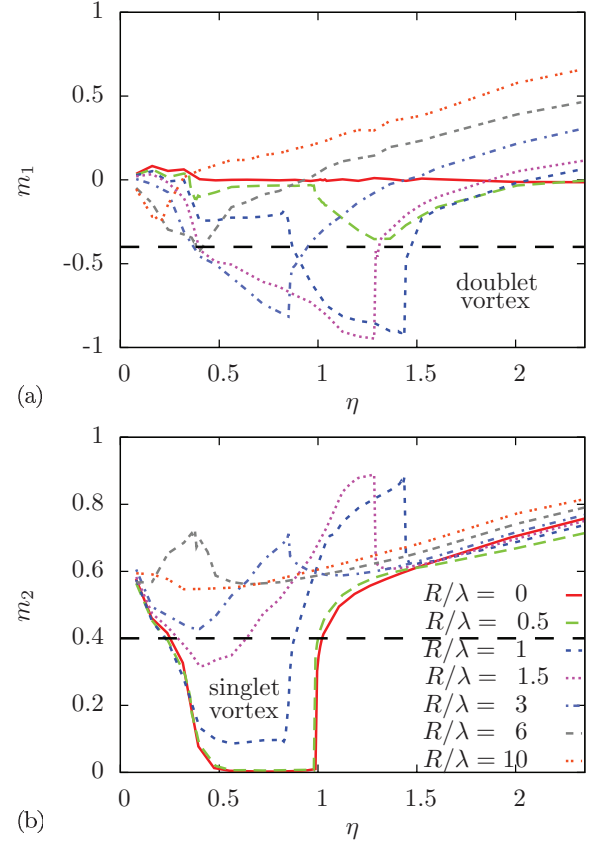


FIG. 3. (Color online) Orientational order parameters (a)  $m_1$  and (b)  $m_2$  for several swimming radii  $R$  as a function of swimmer density  $\eta$ . The horizontal dashed lines represent the criteria for the vortex states.

In the case of no correlation of neighboring rods  $m_1 = 0$  and  $m_2 = 0.5$ . Perpendicular orientation is indicated by  $m_1 = 0$  and  $m_2 = 0$ . A perfect parallel orientation leads to  $m_1 = 1$  and  $m_2 = 1$ , while an antiparallel alignment is represented by  $m_1 = -1$  and  $m_2 = 1$ . Furthermore, we calculate (as a dynamical diagnostics) the mean angular velocity

$$\langle \omega \rangle = \frac{1}{N} \sum_{\alpha=1}^N \dot{\phi}_{\alpha} \quad (15)$$

of the rods.

The dilute state is characterized by almost freely rotating rods with just a few collisions. We define this state by a combination of structural and dynamical criteria demanding that  $m_1 > -0.4$ ,  $m_2 > 0.4$ , and  $\langle \omega \rangle \geq 0.99\omega_0$  should hold in the dilute state. Moreover, the singlet-vortex state is defined via the condition  $m_2 \leq 0.4$ , which brings about strong perpendicular orientation of neighboring rods. Conversely, for doublet vortices we require  $m_1 \leq -0.4$ , indicating that neighboring rods are orientated in an antiparallel way. The slow rotor fluid state is defined by the combined complementary conditions  $m_1 > -0.4$ ,  $m_2 > 0.4$ , and  $\langle \omega \rangle < 0.99\omega_0$ .

Simulation data for the orientational order parameters  $m_1$  and  $m_2$  and the mean angular velocity  $\langle \omega \rangle$  are given in Figs. 3 and 4(a), respectively, as a function of swimmer density  $\eta$  for various swimming radii  $R$ . These plots are consistent with the state diagram shown in Fig. 2(a). In detail, for low densities,

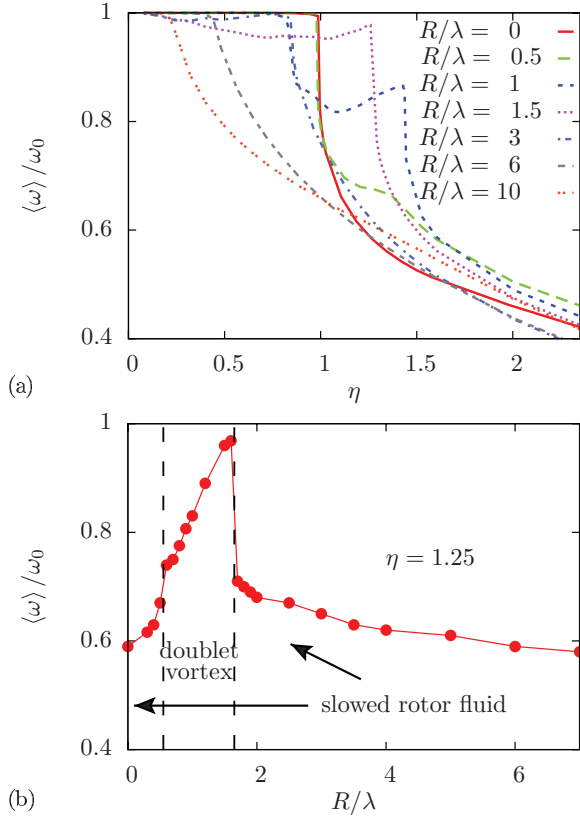


FIG. 4. (Color online) (a) Reduced circular frequency  $\langle \omega \rangle / \omega_0$  as a function of swimmer density  $\eta$  and different rotation radii  $R$ . (b) Reduced circular frequency  $\langle \omega \rangle / \omega_0$  as a function of swimmer radius  $R$  for a fixed swimmer density  $\eta = 1.25$  showing the reentrance of the slowed rotor fluid. The intermediate doublet-vortex state is denoted by vertical dashed lines.

clearly the dilute state emerges. For small radii,  $m_2$  drops down to zero for intermediate densities and then increases again. This demonstrates the occurrence of the singlet-vortex state. At higher densities there is no indication for the doublet-vortex state, but the system goes directly into the slowed rotor fluid state, as indicated by an alignment that leads to the increase of  $m_2$ . This is accompanied by a very sharp reduction in the mean angular velocity as shown in Fig. 4(a).

For  $R > \lambda/2$ , in contrast, there is an overshoot of  $m_2$  as a function of density just after the singlet vortex is stable, implying a parallel ordering of neighboring rods. This points to the new state of doublet vortices. This is simultaneously revealed by a largely negative  $m_1$  as indicative for the antiparallel doublet-vortex state. Again, further increasing of the density leads to the slowed rotor fluid state where the swimmers hinder each other in rotating [see again Fig. 4(a)].

Finally, for very large  $R$ , the dilute to slowed rotor fluid state becomes more and more blurred. For  $R \rightarrow \infty$  the crossover from the dilute to a swarming state [12,26] is approached slowly as observed in Ref. [25].

Figure 4(b) shows the mean angular velocity  $\langle \omega \rangle$  now as a function of the swimming radius  $R$  for fixed density  $\eta = 1.25$ . Clearly  $\langle \omega \rangle$  is nonmonotonic, revealing again the reentrant transition of the slowed rotor fluid phase with an intermediate doublet-vortex phase.

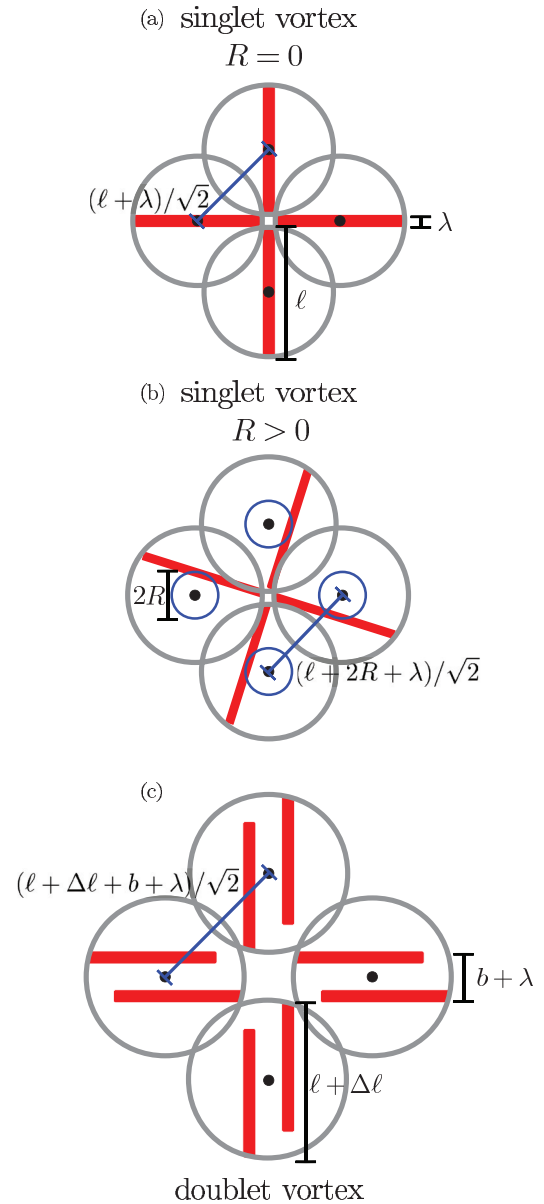


FIG. 5. (Color online) Schematic representations of rod-shaped circle swimmers in the vortex states, showing typical configurations marked in Figs. 2(b) and 2(c). The singlet-vortex state is illustrated for (a) a passive rodlike particle and (b) an active swimmer whose center of mass moves on a circle with radius  $R$ , shown here by small dark (blue) circles. The doublet-vortex state is sketched in (c). In all figures black dots represent the rotation center of the swimmers, while the light gray circles indicate the area covered by the circle swimmers during a full rotation. The lattice constants for all square lattices are given as well.

As a general final remark the order parameter plots Figs. 3 and 4 reveal that some transitions are pretty sharp (in particular the transition from the doublet vortex to the slowed rotor fluid state at low  $R$ ) and other are rather smooth crossovers whose location depends a bit on the precise definition of the states (as for the transition from the doublet vortex to the slowed rotor fluid state at high  $R$ ). We emphasize, however, that the global topology of the state diagram does not change if the transition criteria as shown by the dashed lines in Fig. 3 are modified.

#### IV. SIMPLE THEORY

Let us now present a simple instability theory to predict the state diagram of rodlike circle swimmers. For a vanishing swimming radius  $R$ , as already denoted in Ref. [75], the singlet vortices are mostly governed by a situation where four rodlike circle swimmers on a square lattice rotate with a relative perpendicular orientation [see again the encircled region of the snapshot shown in Fig. 2(c)]. For infinitely thin needles ( $\lambda \rightarrow 0$ ), as sketched in Fig. 5(a), the circles covered by the needle orientation can overlap if the rotating motion is performed coherently with a fixed relative phase shift. The maximal packing fraction that can be reached in this configuration is when needles of length  $\ell$  are placed on a square lattice of lattice constant  $\ell/\sqrt{2}$  [see again Fig. 5(a)], resulting in a threshold packing fraction of

$$\eta_0 = \frac{\pi}{2}. \quad (16)$$

Rods with an effective finite thickness  $\lambda$  need to be more distant to avoid overlap upon their coherent rotation, corresponding to the infinitely thin needles of a larger length  $\ell + \lambda$  [see again Fig. 5(a)]. If they perform an additional circling of swimming radius  $R$  [see Fig. 5(b)], this effective length needs to be augmented by  $2R$  such that the singlet-vortex state should be stable up to

$$\eta_1(R) = \eta_0 \left( \frac{\ell}{\ell + 2R + \lambda} \right)^2. \quad (17)$$

We now employ a similar argument for the doublet-vortex state by considering effective composite rods consisting of a swimmer pair [see Fig. 5(c)]. A suitable cutout from a simulation snapshot is presented in Fig. 2(d). In the simulations, the pairs are observed to rotate around their joint center of mass without exhibiting any circling. The swimmer pair [see the encircled region of the snapshot shown in Fig. 2(d)] possesses typically an interrod distance  $b$  and is laterally shifted by an amount of  $\Delta\ell$  [see again Fig. 5(c)]. In general, these two quantities depend on the prescribed swimming radius  $R$  and the prescribed density  $\eta$ . Lacking any theoretical input for these quantities  $b$  and  $\Delta\ell$ , we resort in our simulation data to determine them and to achieve at least a consistent theory. In detail, we identify swimmer pairs by a center of mass distance less than a cutoff  $r_c$  that we chose in the considered density range as  $r_c = 8\lambda$ . For all identified pairs, we average their mutual distance  $b$  and their lateral shift  $\Delta\ell$ . Results are presented in Fig. 6(a). Interestingly,  $b$  and  $\Delta\ell$  depend strongly on the swimming radius  $R$ , but are rather density independent. In fact, the data obtained for two selected densities  $\eta = 0.75$  and 1 almost coincide. Therefore, we skip the density dependence and consider just  $b(R)$  and  $\Delta\ell(R)$  for which we obtain linear and hyperbolic fits from the simulation data [see dashed lines in Fig. 6(a)] as

$$b(R)/\lambda = 1.73R/\lambda + 0.78/\lambda, \quad (18)$$

$$\Delta\ell(R)/\lambda = 4.29/R/\lambda - 0.93/\lambda. \quad (19)$$

After all one can then treat a pair effectively as a rectangular block of length  $\ell + \Delta\ell(R)$  and width  $b(R) + \lambda$ . Since the block now contains two particles, the instability density for

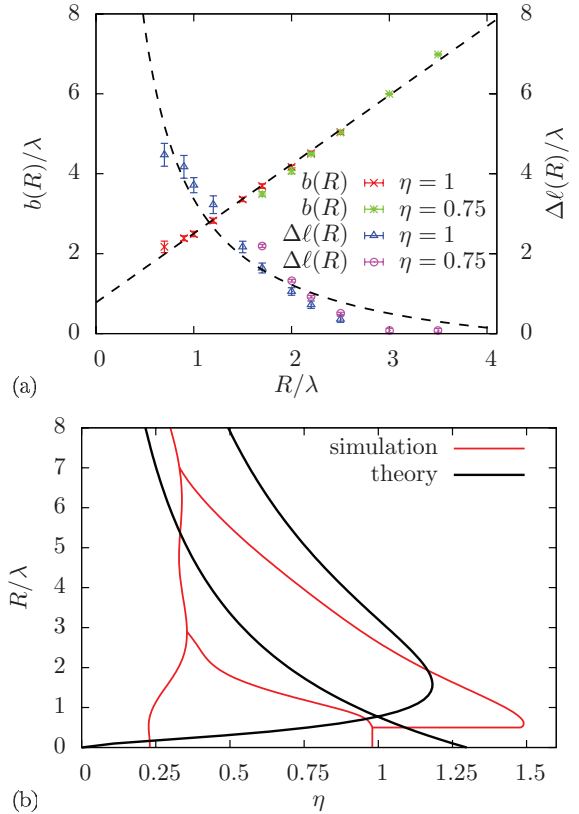


FIG. 6. (Color online) (a) Spatial extent of the circle swimmer pairs in the doublet-vortex state as characterized by the width  $b$  and the extended length  $\Delta\ell$  as a function of the swimming radius  $R$  for different densities  $\eta = 0.75$  and 1. (b) Instability lines for the singlet and doublet-vortex states as obtained from our analysis. The simulated state diagram is shown as a reference.

the doublet-vortex state now reads

$$\eta_2(R) = 2\eta_0 \left( \frac{\ell}{\ell + \Delta\ell(R) + b(R) + \lambda} \right)^2. \quad (20)$$

In Fig. 6(b) both instability lines obtained from either Eq. (17) or (20) are shown. The simulated state diagram from Fig. 2(a) is plotted as a reference. Given the simplifications entering in our instability theory, the transition lines describe the simulation data reasonably well. Moreover, the reentrance effect of the slowed rotor fluid is well captured by our instability analysis such that the topology of the phase diagram is predicted correctly by the theory.

We finally remark that our instability analysis also sheds light on the stability of the singlet- and doublet-vortex states for parameter combinations different from those used in our simulation study. For example, one important condition is that the aspect ratio of the swimmers is high since the reference system in the theory consists of infinitely thin hard needles. This implies that no multiplet-vortex states are expected for almost spherical swimmers.

#### V. CONCLUSION

We have studied the collective dynamical behavior of a simple two-dimensional model of circle-swimming rigid rods

by computer simulation. A different vortex array formation was found where a vortex is composed of a circle swimmer pair, which we referred to as a doublet-vortex state.

The results obtained in our modeling of circle swimmers can be verified in experiments of circle swimmers on two-dimensional substrates. An ideal realization for our model consists of such colloidal rods that are catalytically driven from one side such that they perform strong circular swimming. The swimming radius can in principle be tuned by the lever arm length of the spot where the catalytical reaction happens. The same idea can be used for thermally driven rodlike particles as proposed in Ref. [38]. It is, however, essential to use slender rodlike particles in order to obtain the singlet- and doublet-vortex states. As documented by our theoretical approach, almost spherical particles with a low aspect ratio are not expected to show these vortex states.

For the future, it would be interesting to explore other physical shapes of the swimmer such as recently explored  $L$  particles [64] or  $C$  particles that have a strong tendency to form stacks [91]. We expect that the pairing process will be significantly disturbed for a different particle shape. For such nonconvex particle shapes, it is possible that multiplet-vortex states arise, which comprise an even higher number of swimmers.

Further theoretical efforts should be aimed at expanding the model and equations of motion step by step by considering effects that are relevant in experiment such as multibody hydrodynamic interactions and flexibility of particle shape. The effect of finite temperature could be incorporated as well if one wishes to assess the effect of translation and rotational noise (e.g., tumbling in bacteria) in more detail. In fact, previous studies [75] have already shown that the results are stable with respect to noise provided the strength of the noise is not too large. We have confirmed the stability for some selected parameters also for the doublet-vortex state. It is also desirable to explore the model in three spatial dimensions where the swimming path is a helix rather than a circle [92]. Finally, it would be challenging to construct microscopic theories that are capable of predicting the observed emergent states advanced in this study. Dynamical density functional theory for anisotropic systems [45,93,94] might provide a promising avenue for this.

#### ACKNOWLEDGMENTS

We thank Henricus H. Wensink for helpful discussions. This work was financially supported by the ERC Advanced Grant INTERCOCOS (Grant No. 267499) and by the DFG within SFB TR6 (Project No. D3).

- 
- [1] M. E. Cates, *Rep. Prog. Phys.* **75**, 042601 (2012).
  - [2] M. C. Marchetti, J.-F. Joanny, S. Ramaswamy, J. P. T. B. Liverpool, M. Rao, and R. A. Simha, [arXiv:1207.2929](https://arxiv.org/abs/1207.2929).
  - [3] P. Romanczuk, M. Bär, W. Ebeling, B. Linder, and L. Schimansky-Geier, *Europhys. Lett. Spec. Top.* **202**, 1 (2012).
  - [4] T. Vicsek and A. Zafeiris, *Phys. Rep.* **517**, 71 (2012).
  - [5] J. Toner, Y. H. Tu, and S. Ramaswamy, *Ann. Phys. (NY)* **318**, 170 (2005).
  - [6] M. F. Copeland and D. B. Weibel, *Soft Matter* **5**, 1174 (2009).
  - [7] G. Subramanian, D. L. Koch, and S. R. Fitzgibbon, *Phys. Fluids* **23**, 041901 (2011).
  - [8] A. Sokolov and I. S. Aranson, *Phys. Rev. Lett.* **103**, 148101 (2009).
  - [9] K. Drescher, J. Dunkel, L. H. Cisneros, S. Ganguly, and R. E. Goldstein, *Proc. Natl. Acad. Sci. USA* **108**, 10940 (2011).
  - [10] M. E. Cates, D. Marenduzzo, I. Pagonabarraga, and J. Tailleur, *Proc. Natl. Acad. Sci. USA* **107**, 11715 (2010).
  - [11] D. B. Kearns, *Nat. Rev. Microbiol.* **8**, 634 (2010).
  - [12] S. Ramaswamy, *Annu. Rev. Condens. Matter Phys.* **1**, 323 (2010).
  - [13] S. Thutupalli, R. Seemann, and S. Herminghaus, *New J. Phys.* **13**, 073021 (2011).
  - [14] S. R. McCandlish, A. Baskaran, and M. F. Hagan, *Soft Matter* **8**, 2527 (2012).
  - [15] H. C. Berg, *Phys. Today* **53**(1), 24 (2000).
  - [16] C. Dombrowski, L. Cisneros, S. Chatkaew, R. E. Goldstein, and J. O. Kessler, *Phys. Rev. Lett.* **93**, 098103 (2004).
  - [17] A. Sokolov, I. S. Aranson, J. O. Kessler, and R. E. Goldstein, *Phys. Rev. Lett.* **98**, 158102 (2007).
  - [18] I. H. Riedel, K. Kruse, and J. Howard, *Science* **309**, 300 (2005).
  - [19] D. Saintillan and M. J. Shelley, *Phys. Fluids* **20**, 123304 (2008).
  - [20] H. H. Wensink, J. Dunkel, S. Heidenreich, K. Drescher, R. E. Goldstein, H. Löwen, and J. M. Yeomans, *Proc. Natl. Acad. Sci. USA* **109**, 14308 (2012).
  - [21] X. Chen, X. Dong, A. Be'er, H. L. Swinney, and H. P. Zhang, *Phys. Rev. Lett.* **108**, 148101 (2012).
  - [22] A. Kudrolli, G. Lumay, D. Volfson, and L. S. Tsimring, *Phys. Rev. Lett.* **100**, 058001 (2008).
  - [23] V. Schaller, C. Weber, C. Semmrich, E. Frey, and A. R. Bausch, *Nature (London)* **467**, 73 (2010).
  - [24] A. Czirók, E. Ben-Jacob, I. Cohen, and T. Vicsek, *Phys. Rev. E* **54**, 1791 (1996).
  - [25] H. H. Wensink and H. Löwen, *J. Phys.: Condens. Matter* **24**, 464130 (2012).
  - [26] T. Vicsek, A. Czirók, E. Ben-Jacob, I. Cohen, and O. Shochet, *Phys. Rev. Lett.* **75**, 1226 (1995).
  - [27] G. Miño, T. E. Mallouk, T. Darnige, M. Hoyos, J. Dauchet, J. Dunstan, R. Soto, Y. Wang, A. Rousselet, and E. Clement, *Phys. Rev. Lett.* **106**, 048102 (2011).
  - [28] T. Ishikawa, N. Yoshida, H. Ueno, M. Wiedeman, Y. Imai, and T. Yamaguchi, *Phys. Rev. Lett.* **107**, 028102 (2011).
  - [29] F. G. Woodhouse and R. E. Goldstein, *Phys. Rev. Lett.* **109**, 168105 (2012).
  - [30] J. Schwarz-Linek, C. Valeriani, A. Cacciuto, M. E. Cates, D. Marenduzzo, A. N. Morozov, and W. C. K. Poon, *Proc. Natl. Acad. Sci. USA* **10**, 4052 (2012).
  - [31] D. Volfson, A. Kudrolli, and L. S. Tsimring, *Phys. Rev. E* **70**, 051312 (2004).
  - [32] V. Narayan, S. Ramaswamy, and N. Menon, *Science* **317**, 5834 (2007).
  - [33] M. Garcia, S. Berti, P. Peyla, and S. Rafai, *Phys. Rev. E* **83**, 035301 (2011).

- [34] D. Helbing, I. Farkas, and T. Vicsek, *Nature (London)* **407**, 487 (2000).
- [35] J. Zhang, W. Klingsch, A. Schadschneider, and A. Seyfried, *J. Stat. Mech.* (2012) P02002.
- [36] A. Erbe, M. Zientara, L. Baraban, C. Kreidler, and P. Leiderer, *J. Phys.: Condens. Matter* **20**, 404215 (2008).
- [37] J. Palacci, C. Cottin-Bizonne, C. Ybert, and L. Bocquet, *Phys. Rev. Lett.* **105**, 088304 (2010).
- [38] I. Buttinoni, G. Volpe, F. Kümmel, G. Volpe, and C. Bechinger, *J. Phys.: Condens. Matter* **24**, 284129 (2012).
- [39] R. Dreyfus, J. Baudry, M. L. Roper, M. Fermigier, H. A. Stone, and J. Bibette, *Nature (London)* **437**, 862 (2005).
- [40] A. Snezhko, M. Belkin, I. S. Aranson, and W.-K. Kwok, *Phys. Rev. Lett.* **102**, 118103 (2009).
- [41] A. Snezhko and I. S. Aranson, *Nat. Mater.* **10**, 698 (2011).
- [42] G. Rückner and R. Kapral, *Phys. Rev. Lett.* **98**, 150603 (2007).
- [43] M. N. Popescu, S. Dietrich, and G. Oshanin, *J. Chem. Phys.* **130**, 194702 (2009).
- [44] F. Peruani, A. Deutsch, and M. Bär, *Phys. Rev. E* **74**, 030904 (2006).
- [45] H. H. Wensink and H. Löwen, *Phys. Rev. E* **78**, 031409 (2008).
- [46] Y. Yang, V. Marceau, and G. Gompper, *Phys. Rev. E* **82**, 031904 (2010).
- [47] F. Ginelli, F. Peruani, M. Bär, and H. Chaté, *Phys. Rev. Lett.* **104**, 184502 (2010).
- [48] N. Sambelashvili, A. W. C. Lau, and D. Cai, *Phys. Lett. A* **360**, 507 (2007).
- [49] A. M. Menzel, *Phys. Rev. E* **85**, 021912 (2012).
- [50] H. C. Berg and L. Turner, *Biophys. J.* **58**, 919 (1990).
- [51] W. R. DiLuzio, L. Turner, M. Mayer, P. Garstecki, D. B. Weibel, H. C. Berg, and G. M. Whitesides, *Nature (London)* **435**, 1271 (2005).
- [52] E. Lauga, W. R. DiLuzio, G. M. Whitesides, and H. A. Stone, *Biophys. J.* **90**, 400 (2006).
- [53] J. Hill, O. Kalkanci, J. L. McMurry, and H. Koser, *Phys. Rev. Lett.* **98**, 068101 (2007).
- [54] V. B. Shenoy, D. T. Tambe, A. Prasad, and J. A. Theriot, *Proc. Natl. Acad. Sci. USA* **104**, 8229 (2007).
- [55] S. Schmidt, J. van der Gucht, P. M. Biesheuvel, R. Weinkamer, E. Helfer, and A. Frey, *Eur. Biophys. J.* **37**, 8229 (2008).
- [56] S. B. Babu and H. Stark, *New J. Phys.* **14**, 085012 (2012).
- [57] Y. Sumino, K. H. Nagai, Y. Shitaka, D. Tanaka, K. Yoshikawa, H. Chaté, and K. Oiwa, *Nature (London)* **48**, 448 (2012).
- [58] D. M. Woolley, *Reproduction* **216**, 259 (2003).
- [59] B. M. Friedrich and F. Jülicher, *New J. Phys.* **10**, 123035 (2008).
- [60] R. Mach and F. Schweitzer, *Bull. Math. Biol.* **69**, 539 (2007).
- [61] S. Nakata, Y. Iguchi, S. Ose, M. Kuboyama, T. Ishii, and K. Yoshikawa, *Langmuir* **13**, 4454 (1997).
- [62] T. Ohta and T. Ohkuma, *Phys. Rev. Lett.* **102**, 154101 (2009).
- [63] G. Volpe, I. Buttinoni, D. Vogt, H.-J. Kümmerer, and C. Bechinger, *Soft Matter* **7**, 8810 (2011).
- [64] F. Kümmel, B. ten Hagen, R. Wittkowski, I. Buttinoni, C. Bechinger, and H. Löwen, [arXiv:1302.5787](https://arxiv.org/abs/1302.5787).
- [65] A. Reinmüller, H. J. Schöpe, and T. Palberg, *Langmuir* **29**, 1738 (2013).
- [66] S. van Teeffelen and H. Löwen, *Phys. Rev. E* **78**, 020101 (2008).
- [67] S. van Teeffelen, U. Zimmermann, and H. Löwen, *Soft Matter* **5**, 4510 (2009).
- [68] B. ten Hagen, S. van Teeffelen, and H. Löwen, *J. Phys.: Condens. Matter* **23**, 194119 (2011).
- [69] P. K. Radtke and L. Schimansky-Geier, *Phys. Rev. E* **85**, 051110 (2012).
- [70] M. Tarama and T. Ohta, *J. Phys.: Condens. Matter* **24**, 464129 (2012).
- [71] J. Dunstan, G. Miño, E. Clement, and R. Soto, *Phys. Fluids* **24**, 011901 (2012).
- [72] R. Ledesma-Aguilar, H. Löwen, and J. M. Yeomans, *Eur. Phys. J. E* **35**, 9746 (2012).
- [73] T. Si, *Physica A* **391**, 3054 (2012).
- [74] T. Kirchhoff, H. Löwen, and R. Klein, *Phys. Rev. E* **53**, 5011 (1996).
- [75] R. Kirchhoff and H. Löwen, *Europhys. Lett.* **69**, 291 (2005).
- [76] R. Kirchhoff and H. Löwen, *J. Phys.: Condens. Matter* **17**, 7805 (2005).
- [77] M. Sullivan, K. Zhao, C. Harrison, R. H. Austin, M. Megens, A. Hollingsworth, W. B. Russel, Z. Cheng, T. Mason, and P. M. Chaikin, *J. Phys.: Condens. Matter* **15**, S11 (2003).
- [78] Z. Cheng, P. M. Chaikin, and T. G. Mason, *Phys. Rev. Lett.* **89**, 108303 (2002).
- [79] A. I. Bishop, T. A. Nieminen, N. R. Heckenberg, and H. Rubinsztein-Dunlop, *Phys. Rev. A* **68**, 033802 (2003).
- [80] Y. Fily, A. Baskaran, and M. C. Marchetti, *Soft Matter* **8**, 3002 (2012).
- [81] L. H. Cisneros, R. Cortez, C. Dombrowski, R. E. Goldstein, and J. O. Kessler, *Phys. Fluids* **43**, 737 (2007).
- [82] C. W. Wolgemuth, *Biophys. J.* **95**, 1564 (2008).
- [83] A. Kaiser, H. H. Wensink, and H. Löwen, *Phys. Rev. Lett.* **108**, 268307 (2012).
- [84] H. Löwen, *Phys. Rev. Lett.* **72**, 424 (1994).
- [85] H. Löwen, *J. Chem. Phys.* **100**, 6738 (1994).
- [86] H. Graf and H. Löwen, *Phys. Rev. E* **59**, 1932 (1999).
- [87] E. Allahyarov and H. Löwen, *Phys. Rev. E* **62**, 5542 (2000).
- [88] E. Allahyarov, H. Löwen, and G. Gompper, *Phys. Rev. E* **68**, 061903 (2003).
- [89] M. M. Tirado, C. L. Martinez, and J. G. de la Torre, *J. Chem. Phys.* **81**, 2047 (1984).
- [90] See Supplemental Material at <http://link.aps.org/supplemental/10.1103/PhysRevE.87.032712> for movies showing the occurring states.
- [91] M. Marechal, R. J. Kortschot, A. F. Demirörs, A. Imhof, and M. Dijkstra, *Nano Lett.* **10**, 1907 (2010).
- [92] R. Wittkowski and H. Löwen, *Phys. Rev. E* **85**, 021406 (2012).
- [93] M. Rex, H. H. Wensink, and H. Löwen, *Phys. Rev. E* **76**, 021403 (2007).
- [94] R. Wittkowski and H. Löwen, *Mol. Phys.* **109**, 2935 (2011).